(Received 4 March 2025, Accepted 10 April 2025, Scheduled 16 April 2025)

A Dual-Port Millimeter-Wave Frequency Reconfigurable Array Antenna

Mingming Gao[1,2], Hang Yuan[1,2,*], Jingchang Nan[1,2], Hongliang Niu[1,2], and Chang Ge[1,2]

[1]*Liaoning Technical University, China*
[2]*Liaoning Key Laboratory of Radio Frequency and Big Data for Intelligent Applications, China*

ABSTRACT: With the advancement of millimeter wave communication technology, reconfigurable antennas have garnered significant attention due to their adaptability. However, their radiation gain and sidelobe suppression performance are often constrained by factors such as diode package size and array scale. To address these challenges, this paper proposes a three-state frequency reconfigurable array antenna with high gain and low sidelobe characteristics, specifically designed to meet the demands of millimeter-wave communication. By optimizing the feed network and radiating element design, the proposed antenna achieves enhanced gain and improved sidelobe suppression. The design employs a dual-port feeding architecture that integrates a Taylor non-uniform amplitude distribution with a series-parallel hybrid feed network. This configuration ensures phase consistency while minimizing the number of diodes to just four, significantly reducing insertion loss and structural complexity. The antenna prototype is fabricated using standard printed circuit board (PCB) technology, with overall dimensions of $60.4 \times 63 \times 0.508\,\text{mm}^3$. Measurement results indicate that the antenna exhibits an impedance bandwidth spanning from 27.5 GHz to 28.5 GHz and from 34.5 GHz to 35.5 GHz. The corresponding peak gains are 19.69 dBi and 19.51 dBi, with the sidelobe levels of 18.93 dB and 18.03 dB, respectively. The proposed antenna demonstrates excellent radiation characteristics and significantly enhances radiation efficiency. With its simple structure, dual-band radiation capability, high gain, and low sidelobe levels, this antenna is highly suitable for millimeter-wave wireless communication systems. It offers a high-performance solution for multi-band communication in 5G/6G networks.

1. INTRODUCTION

With the continuous growth in demand for high data rates and low latency in 5G/6G networks, millimeter-wave frequency band has become a research focus due to its wide bandwidth characteristics [1–3]. The high integration of millimeter-wave devices further accelerates their practical implementation in communication systems. However, conventional fixed-frequency antennas struggle to accommodate dynamic spectrum allocation, thereby limiting the deployment flexibility of millimeter-wave networks. To address this challenge, reconfigurable millimeter-wave array antennas enable the adjustment of operating frequencies, such as 28 GHz and 35 GHz, to meet evolving communication demands. This innovative design is expected to play a crucial role in overcoming the frequency efficiency bottlenecks. Moreover, this research not only improves the performance of existing communication systems but also lays the foundation for future 6G networks, driving the development of more efficient communication technologies and supporting the construction of an intelligent and digital society [4, 5].

In the field of frequency reconfigurable technology, control schemes based on PIN diodes are widely adopted due to their advantages, including low cost and high response speed (< 10 ns) [6]. However, the parasitic effects of diodes at millimeter-wave frequencies can significantly degrade the transmission efficiency of the feed network, thereby limiting the array size and reducing the antenna radiation gain. This degradation poses challenges for both engineering and commercial applications. To address this bottleneck, this research proposes the use of multi-port excited antennas, with PIN diodes serving as switches to control the excitation of the antenna array. This approach reduces the number of switching devices compared to traditional designs, providing a novel paradigm for the development of large-scale reconfigurable arrays [7–16]. Ref. [7] presents a dual-port printed monopole antenna. By controlling four PIN diodes, the radiation mode is modulated, allowing a switch between two distinct modes. In [8], a dual-port 1×2 antenna array is introduced that incorporates a parasitic element surface at the front of the array to generate different radiation patterns, thereby achieving reconfigurability. Compared with radio frequency (RF) switches, the dual-port design provides more effective control over the radiation. Ref. [9] proposes a frequency-reconfigurable array antenna operating in the 3.36–3.7 GHz and 5–5.8 GHz bands, where PIN diodes are used to switch among three operational modes. In [10], a reconfigurable antenna is designed with two driving ports and a sub-wavelength reconfigurable metallic line that shapes the radiation beam; the state of the metallic line is further controlled by 20 PIN diodes, enabling reconfigurability. Ref. [11] describes a dual-port dual-band reconfigurable antenna: when port 1 is powered, the antenna exhibits an omnidirectional radiation pattern in the 5.59–6.04 GHz range, and

* Corresponding author: Hang Yuan (yh1721163227@126.com).

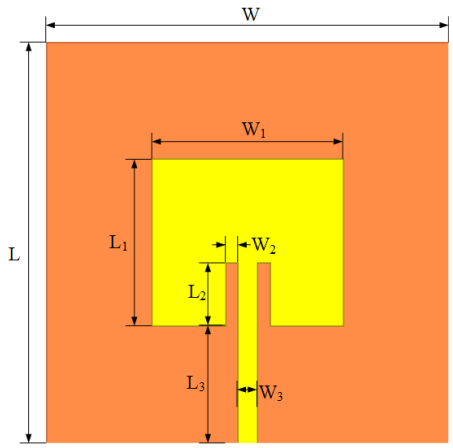

FIGURE 1. Antenna element.

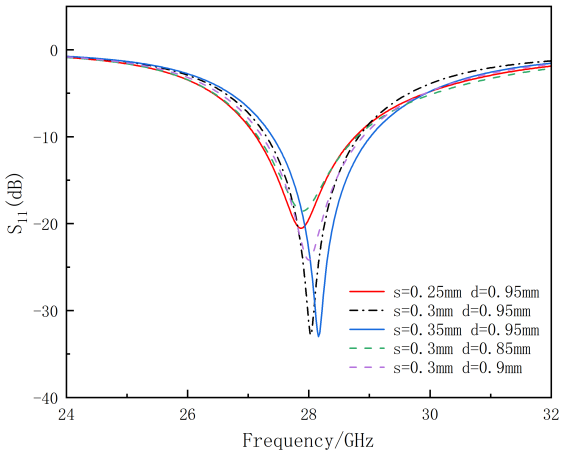

FIGURE 2. Feeder slot parameter.

when port 2 is powered, an end-fire radiation pattern is achieved in the 5.63–6.14 GHz band. Lastly, [14] introduces a reconfigurable antenna operating in the 25–30 GHz range; by controlling the bias state of its units, different operational modes are achieved, although the maximum gain is limited to 4 dBi.

Millimeter-wave array antennas face two major challenges in practical applications: environmental sensitivity and elevated sidelobe levels [17]. Atmospheric absorption and dense multipath effects lead to significant signal fading, while the low sidelobe levels of traditional uniform arrays further degrade communication quality. To address these issues, this study optimizes the element excitation distribution using the Taylor synthesis method, combined with a reconfigurable feed network to achieve dynamic matching for dual frequency bands (28 GHz and 35 GHz). Theoretically, this design suppresses sidelobe levels to below -20 dB while enhancing the system's robustness against environmental disturbances. This approach offers an innovative solution for millimeter-wave communications in high-density urban environments and complex climatic conditions, achieving a balance between high gain and low interference.

This study employs microstrip patch antennas as array elements and develops a tristate millimeter-wave frequency reconfigurable array antenna with high gain and low sidelobes. PIN diodes are integrated into the antenna feed network, and the frequency states of the array are controlled through a bias circuit to achieve tristate reconfigurability. The antenna array is designed using an unequal-amplitude Taylor distribution function and a series-parallel feeding network, resulting in a millimeter-wave microstrip array antenna with enhanced radiation performance. Experimental results demonstrate that the antenna operates effectively in the 27.5 GHz to 28.5 GHz and 34.5 GHz to 35.5 GHz frequency bands, with relative bandwidths of 3.5% and 2.8%, respectively. The measured peak gains in these two bands are 19.69 dBi and 19.46 dBi, with sidelobe levels of 18.68 dB and 18.41 dB, respectively.

The structure of this paper is as follows. Section 2 discusses the overall design of the antenna, analyzing the underlying principles for achieving high gain and low sidelobe levels, as well as the reconfigurable operating mechanism and its implementation. Section 3 presents the research results and compares them with existing studies. Section 4 concludes the paper and outlines future research directions.

2. ANTENNA DESIGN AND ANALYSIS

2.1. Antenna Element Design

This study employs microstrip patch antennas as array elements, designed on a single layer dielectric substrate (Rogers 4350B) with specific material properties: a dielectric constant (ϵ_0) of 3.48, the tangent of dielectric loss ($\tan\delta$) of 0.0009, and a thickness of 0.508 mm, as shown in Fig. 1.

The design of a microstrip antenna begins with the selection of an appropriate dielectric substrate. Once the dielectric constant of the substrate is determined, the substrate thickness h must be further defined. Typically, h follows the approximate formula given in Equation (1) [18]:

$$h \leq \frac{0.5c}{2\pi f_u \sqrt{\epsilon_0}} \tag{1}$$

where c represents the speed of light in a vacuum, f_u the maximum frequency of the antenna's operating band, and ϵ_0 the dielectric constant of the substrate. After calculating the initial value, the actual dielectric substrate thickness is selected as 0.508 mm, considering the processing constraints of the substrate.

The S parameters of the antenna element are mainly influenced by the length d and width s of the slots on both sides of the feed line. Fig. 2 presents the analysis results of the slot length variations and their impact on the feed line performance.

As shown in Fig. 2, the resonant frequency of the antenna element varies with the length (d) and width (s) of the feed line slots. When the width (s) is fixed, an increase in length (d) shifts the resonant frequency toward higher frequencies. Similarly, when the length (d) is fixed, an increase in width (s) also results in a higher resonant frequency. When the slot dimensions are set to $d = 0.95$ mm and $s = 0.3$ mm, the resonant

frequency of the curve is 28 GHz, which corresponds to the optimal value of S_{11} for the antenna element. A similar trend is observed for the antenna element operating at 35 GHz.

2.2. Feed Network Design

To compensate for the high path loss in millimeter-wave signal propagation, this section designs a high-gain array antenna based on the antenna unit described in Section 2.1. Taking the 28 GHz frequency band as an example, the peak gain of a single element is 6.7 dBi. As the number of antenna elements doubles, the gain increases by approximately 3 dBi. With a 32-element array and an optimized feed network loss factor below 0.8 dB, the theoretical gain can reach 21.1 dBi. Additionally, a hybrid series-parallel feeding scheme is introduced. Compared to the traditional series feeding method, this approach improves antenna array layout efficiency and lowers feed network losses [19].

To effectively suppress sidelobe levels, the Taylor synthesis method is employed for array optimization. The key advantage of this method lies in its ability to mitigate abrupt excitation amplitude variations, which are commonly encountered in traditional array synthesis. To account for potential losses during the design process, the sidelobe level is set to -20 dB. The number of elements in the linear array is determined to be eight. The Taylor function is implemented in MATLAB to calculate the current amplitudes for each port, which are then used to design the feed network, resulting in a 4×8 antenna array, as shown in Fig. 3.

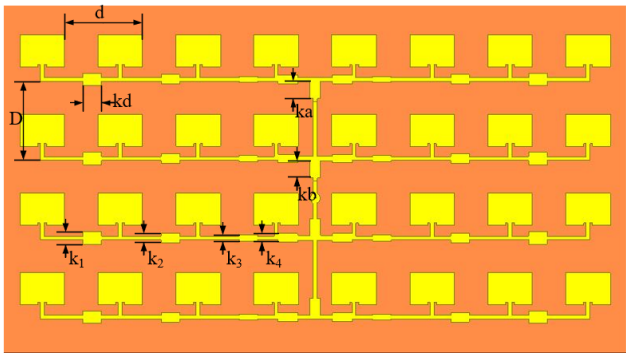

FIGURE 3. 4×8 antenna array.

Within this configuration, the 1×8 linear array functions as a side-fire array. To prevent the occurrence of grating lobes, the element spacing must satisfy the condition λ_g (the guided wavelength at the antenna's operating frequency). Considering mutual coupling effects and antenna size constraints, the optimal element spacing d is further fine-tuned using HFSS to ensure optimal impedance matching and radiation characteristics of the linear array.

As shown in Fig. 4, the S-parameters of the linear array at different element spacings indicate that the element spacing (d) significantly influences the resonance characteristics of the array. When $d = 5.3$ mm, the resonance frequency is 27.14 GHz, with a resonance depth of -32.38 dB. When $d = 6.3$ mm, the resonance frequency shifts to 28 GHz, achieving a deeper resonance of -38.3 dB. When $d = 7.3$ mm, the resonance frequency is 28.9 GHz, and the resonance depth is -31.65 dB. After comparison, an element spacing of $d = 6.3$ mm is selected as it offers the optimal impedance matching for the linear array. The same approach is applied to the 35 GHz linear array design.

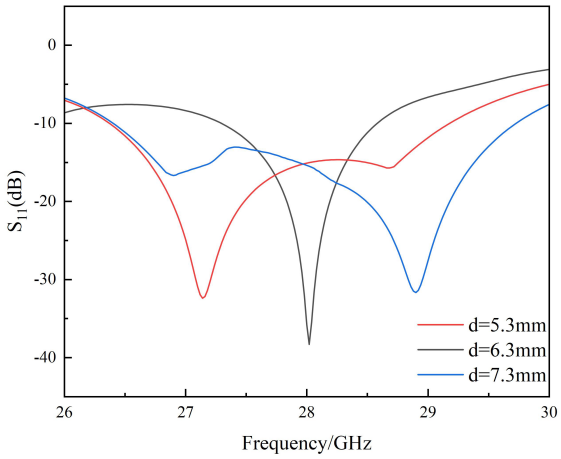

FIGURE 4. 28 GHz linear array element spacing.

In the design of the planar array, the simulation results for the 28 GHz antenna array indicate that the antenna gain can reach 20 dBi. However, the 35 GHz antenna array does not initially meet design expectations. Further investigation reveals that adjusting the distance (D) between the linear arrays can enhance the antenna gain to 20 dBi. After comparison, it is found that a linear array spacing following an arithmetic progression (with the middle spacing being 5.3 ± 0.3 mm) yields the desired performance, as shown in Fig. 5.

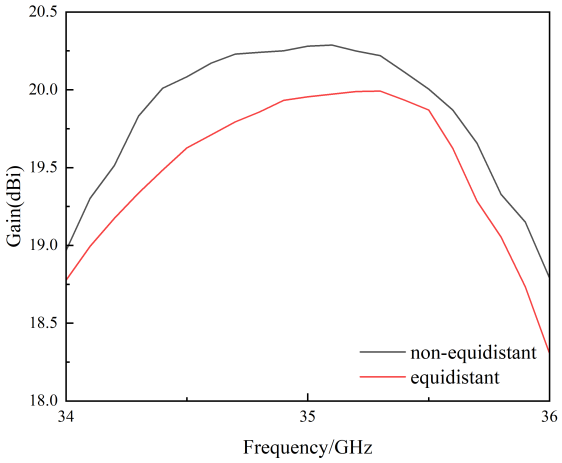

FIGURE 5. 35 GHz linear array spacing.

Table 1 presents the optimal values of the antenna array parameters obtained through HFSS simulation optimization, including the design parameters for both the 28 GHz and 35 GHz antenna arrays.

2.3. Reconfigurable Design

In the design of reconfigurable antennas, in addition to the antenna's main structure, it is also essential to design a DC bias

TABLE 1. Dimensions of the proposed antenna (28 GHz/35 GHz).

Parameters	Values (mm)	Parameters	Values (mm)
W	6.3/6	d	6.3/6
W_1	3.6/2.5	D (Middle spacing)	6.4/5.3
W_2	0.2/0.25	ka	1.4/1
W_3	0.3/0.3	kb	1.35/1.2
L	6.3/6	kd	$\lambda_g/4$
L_1	2.58/2.13	k_1	1
L_2	0.2/0.5	k_2	0.78/0.8
L_3	0.86/1	k_3	0.48/0.7
h	0.508	k_4	0.7/0.4

circuit that has minimal impact on the antenna's radiation characteristics. This is a key challenge in the design of reconfigurable antennas. Typically, achieving tunable antenna performance requires RF switches, which in turn necessitate a DC bias. Since capacitors have the effect of blocking DC while allowing AC to pass, a suitable capacitor component is typically required to prevent DC from entering the RF transmission circuit. Similarly, to prevent RF signals from entering the DC bias network, an inductor is typically used as an RF choke, effectively blocking RF signals while allowing DC to pass. The RF switch and bias circuit integrated into the antenna are shown in Fig. 6.

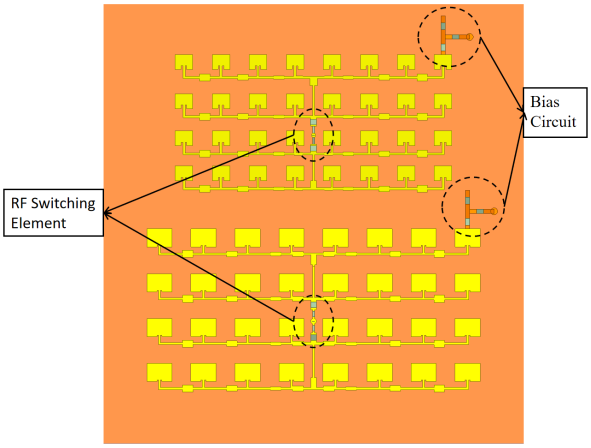

FIGURE 6. The position of RF switch and bias circuit on the antenna.

The PIN diode enables the control of microwave signal transmission and switching due to its distinct electrical characteristics: it exhibits a conductive state under a DC forward bias and a cutoff state under a DC reverse bias. As shown in Fig. 7(a), when the PIN diode is forward biased, it behaves as an equivalent 4 Ω resistor. As shown in Fig. 7(b), when the PIN diode is reverse biased, the diode is equivalent to a parallel combination of a 4 kΩ resistor and a 0.025 pF capacitor.

In the design of reconfigurable antennas, the coupling effect between the RF signal and DC bias can significantly degrade

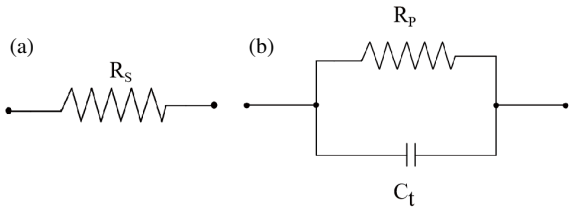

FIGURE 7. Equivalent circuit of the PIN diode: (a) Forward bias; (b) Reverse bias.

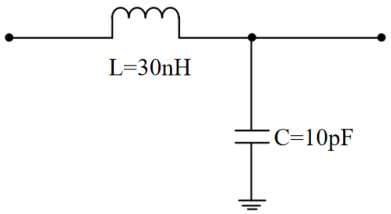

FIGURE 8. Low pass filter circuit.

the antenna's radiation characteristics. To achieve effective isolation, this study employs the low-pass filter network shown in Fig. 8, which consists of a 30 nH surface-mount inductor, a 10 pF capacitor, and a metallized via. The series inductor suppresses RF signal leakage to the DC source by leveraging its high impedance at high frequencies, while the parallel capacitor provides a low-impedance path for the DC bias, utilizing its short-circuiting properties at low frequencies to achieve RF decoupling.

During practical testing, an external +5 V DC bias voltage is required to ensure the proper operation of the circuit components. To prevent excessive forward bias current through the diode, which could lead to device breakdown, a 20 Ω resistor is incorporated into the biasing line to regulate the maximum current under the applied voltage.

The antenna prototype was fabricated, and the sample is shown in Fig. 9.

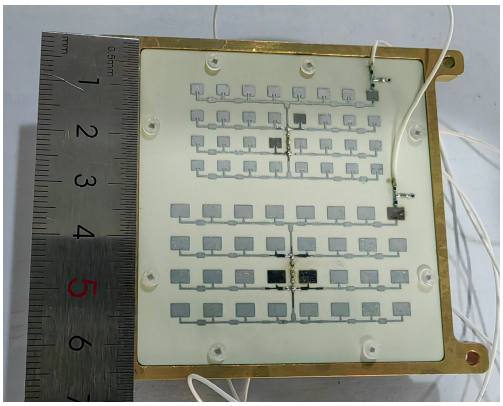

FIGURE 9. Antenna physical picture.

3. MEASUREMENT RESULTS AND DISCUSSION

We performed simulation and practical measurement analysis on the designed antenna. The key parameters analyzed include

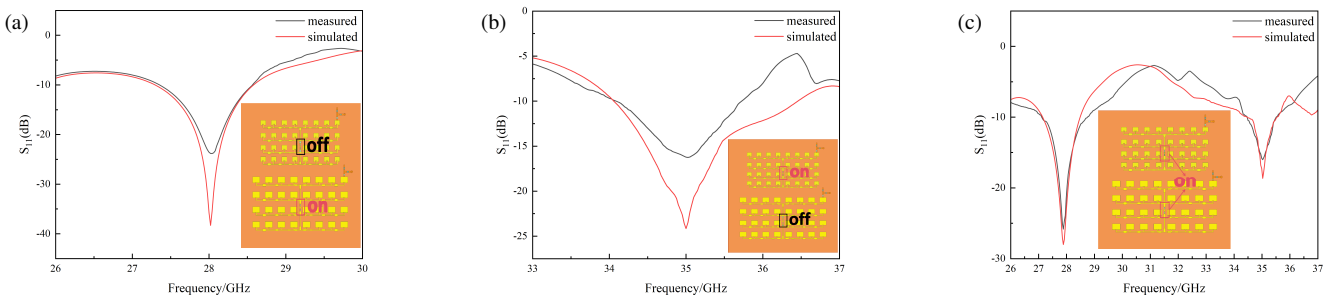

FIGURE 10. Antenna S_{11} measurement and simulation: (a) Mode 1; (b) Mode 2; (c) Mode 3.

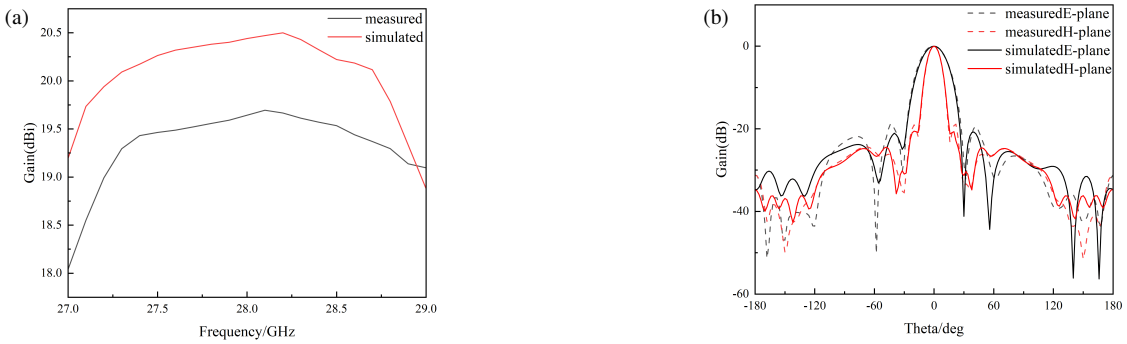

FIGURE 11. Mode 1 measured and simulated: (a) Gain frequency responses, (b) Radiation characteristics.

S_{11}, gain in each operational mode, and sidelobes. The S_{11} plot primarily describes the return loss: for any antenna, the effective return loss value is less than -10 dB. As shown in Fig. 10, the S_{11} of each mode within the target frequency band in both simulation and measurements meets the design requirements. The differences between the simulation and measurement results may be attributed to losses in the PIN diode and other circuit components, minor manufacturing deviations, and the surface roughness of the metal. These factors can significantly impact the antenna's bandwidth and overall performance.

3.1. Mode 1

Figure 11 presents the gain and radiation characteristics of the antenna in Mode 1 (as shown in Fig. 10(a), the PIN diodes of the 28 GHz antenna array are in a closed state, while the PIN diodes of the 35 GHz antenna array are in an open state) within the 27.5–28.5 GHz frequency range, including both simulated and measured results. As shown in Fig. 11(a), the simulated and measured antenna gains are 20.49 dBi and 19.69 dBi, respectively, with a difference of 0.8 dBi. The measured gain remains above 19.5 dBi across the operating frequency band. The results indicate that at lower frequencies, the measured and simulated gain trends are closely aligned. However, at higher frequencies, the measured gain curve appears smoother than the simulated one. This discrepancy is primarily attributed to mutual coupling effects in the array at high frequencies. In practice, mutual coupling reduces gain fluctuations through energy leakage and phase disturbances, resulting in a smoother measured curve. As shown in Fig. 11(b), the simulated and measured sidelobe levels in the E-plane are 20.58 dB and 18.93 dB, respectively, while in the H-plane, the simulated and measured results are 20.78 dB and 20.43 dB, respectively. The measured sidelobe levels remain above 18.9 dB across the operating frequency band, indicating that the main lobe of the antenna maintains consistency, with the radiated energy effectively concentrated in the intended transmission direction, as expected in the design.

3.2. Mode 2

Figure 12 presents the gain and radiation characteristics of the antenna in Mode 2 (as shown in Fig. 10(b), and the PIN diodes of the 28 GHz antenna array are in a open state, while the PIN diodes of the 35 GHz antenna array are in an closed state) within the 34.5–36.5 GHz frequency range, including both simulated and measured results. In Fig. 12(a), the simulated and measured antenna gains are 20.28 dBi and 19.51 dBi, respectively, with a difference of 0.77 dBi. The measured gain remains above 19.5 dBi across the operating frequency band. The gain curve shows that while the measured and simulated results follow a similar trend, there is an offset, primarily attributed to transmission losses in the feed network and the non-ideal characteristics of the diodes. As shown in Fig. 12(b), the simulated and measured sidelobe levels in the E-plane are 20.17 dB and 18.97 dB, respectively, while in the H-plane, the simulated and measured values are 18.17 dB and 18.03 dB, respectively. The measured sidelobe levels remain above 18 dB throughout the operating frequency band, indicating that in Mode 2, the antenna energy is effectively concentrated in the main lobe direction, providing strong interference resistance, similar to the performance observed in Mode 1.

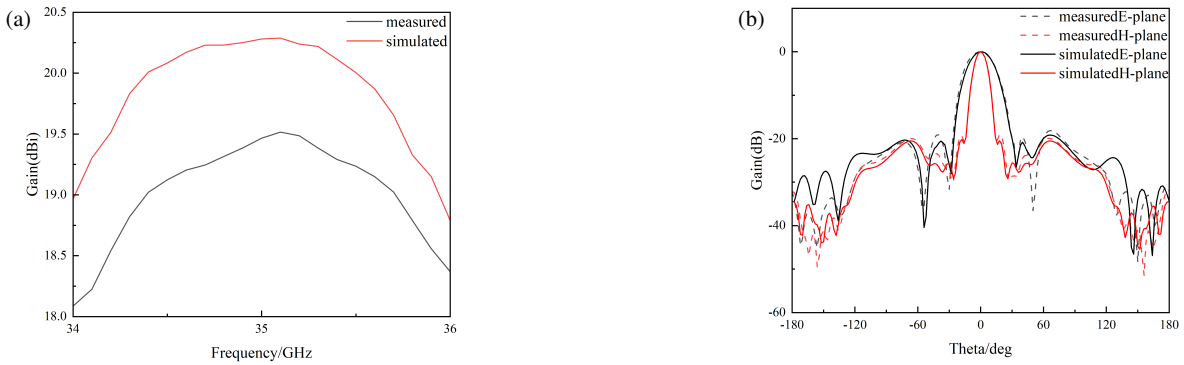

FIGURE 12. Mode 2 measured and simulated: (a) Gain frequency response; (b) Radiation characteristics.

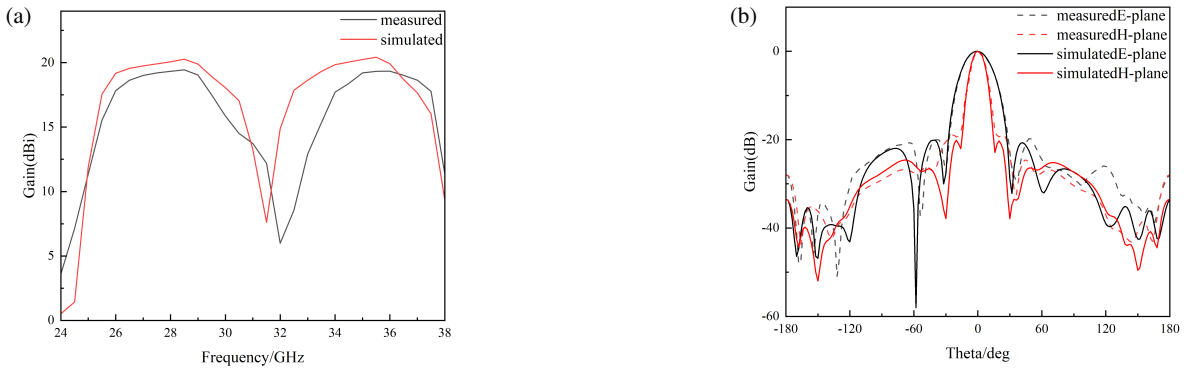

FIGURE 13. Mode 3 measured and simulated: (a) Gain frequency response; (b) Radiation characteristics.

3.3. Mode 3

Figure 13 presents the gain and radiation characteristics of the antenna in Mode 3 (as shown in Fig. 10(c), the PIN diodes of both the 28 GHz and 35 GHz antenna arrays are fully closed) for the frequency ranges 27.5–28.5 GHz and 34.5–36.5 GHz, including both simulated and measured results. As shown in Fig. 13(a), the simulated and measured antenna gains are 20.42 dBi and 19.44 dBi, respectively, with a difference of 0.98 dBi. The measured gain remains above 19.4 dBi across the operating frequency band. The results indicate that in the lower frequency range, the measured gain curve closely follows the simulated trend. However, in the higher frequency range, a noticeable frequency offset is observed. This discrepancy is primarily attributed to the higher sensitivity of the high-frequency radiation elements to external environmental factors during testing, as well as the misalignment of the standard horn antenna used in the measurement setup, which caused the frequency shift in the high-frequency gain curve. Fig. 13(b) shows sidelobe levels of the antenna. In the E-plane, the simulated and measured sidelobe levels are 20.81 dB and 18.96 dB, respectively, while in the H-plane, the simulated and measured values are 20.09 dB and 19.97 dB, respectively. The measured sidelobe levels remain above 18.9 dB across the operating frequency band. The results indicate that the radiation characteristic curve of Mode 3 exhibits greater distortion than Modes 1 and 2, primarily due to its dual-frequency operation. Nevertheless, the antenna effectively concentrates its transmitted energy in the main lobe direction, maintaining the desired radiation performance.

Figure 14 presents the simulated and measured results of port isolation in this state. As observed in the figure, the antenna port isolation remains below −35 dB, indicating that during dual-band operation, the signal interference between the antenna ports is minimal, and there is no significant crosstalk between them. This result confirms that the antenna design effectively minimizes interference and ensures proper isolation between the ports, which is essential for preserving the integrity of the communication signal, particularly in multi-frequency applications.

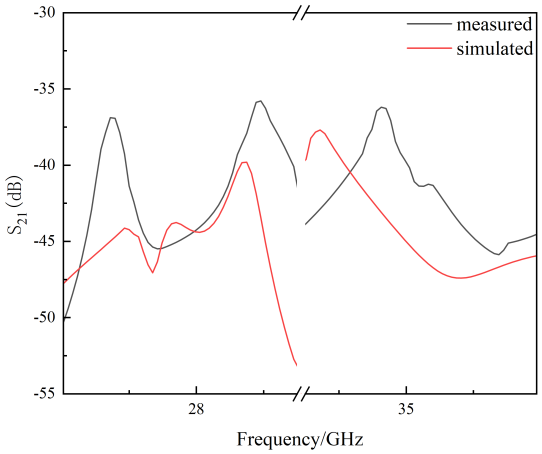

FIGURE 14. Mode 3 S_{21} measurement and simulation.

TABLE 2. Comparison of the proposed antenna with previously reported antennas.

Reference	Port numbers	PIN diode	Frequency/GHz	Gain/dBi	Number of Modes	Size/mm^3
[7]	2	4	2.49–2.69	3.9	2	$134 \times 129 \times 2$
[9]	2	4	3.36–3.7/5–5.8	2.2/3	3	$48.5 \times 25 \times 1.6$
[10]	2	20	3.4–3.8	9.3	2	$80 \times 80 \times 18.7$
[13]	2	2	2.7–5.6	1.8–3.26	2	$45 \times 65 \times 1.6$
[14]	2	2	25–30	4	4	$30 \times 23 \times 0.25$
[15]	1	8	27.5–28.5	11.2–19.2	3	-
This paper	2	4	27.5–28.5/34.5–35.5	19.69/19.51	3	$60.4 \times 63 \times 0.508$

The key performance metrics of the frequency reconfigurable array antenna designed in this study were compared with those of antennas reported in the literature, as summarized in Table 2. Refs. [7, 9, 10, 13] achieved reconfigurable antenna designs below 6 GHz; however, the antennas in [7, 10] are large in volume and height, making integration with planar circuits challenging. Additionally, the gain of the antennas in [9, 13] is relatively low. Refs. [14, 15] implemented reconfigurable antenna designs at higher frequencies; however, the antenna in [14] exhibits lower gain, while the design in [15] requires a larger number of diodes than the antenna proposed in this study. In terms of antenna structure, gain, and frequency metrics, the antenna designed in this study outperforms similar models, achieving a frequency-reconfigurable array antenna with high gain and low sidelobes in the millimeter-wave band.

The physical model and testing environment are shown in Fig. 15.

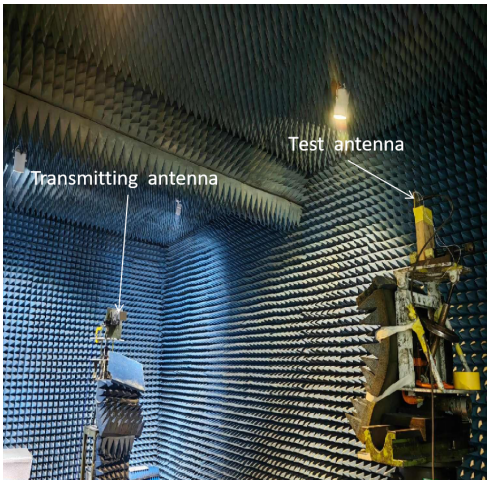

FIGURE 15. The picture of antenna far-field measurement.

4. CONCLUSION

This paper presents a three-state frequency-reconfigurable array antenna with high gain and low sidelobe levels. It provides a comprehensive overview of the design process, from the development of the antenna element design to the analysis of its operating principles and the implementation of the reconfigurable array antenna. By controlling RF switches, the antenna's radiation characteristics can be adjusted, enabling different operational states within the frequency bands of 27.5 GHz–28.5 GHz and 34.5 GHz–35.5 GHz. Within these operating frequency bands, the antenna achieves peak gains of 19.69 dBi and 19.51 dBi, respectively, with sidelobe levels of 18.93 dB and 18.03 dB. Featuring a simple structure, high radiation gain, and low sidelobe levels, the proposed antenna is well suited for millimeter-wave communication systems.

ACKNOWLEDGEMENT

This work was supported by the Applied Basic Research of Liaoning Province (2022JH2/101300275), Basic Scientific Research Project of Education Department of Liaoning Province (JYTMS20230818), and the National Natural Science Foundation of China (61971210).

REFERENCES

[1] Di Renzo, M., A. Zappone, M. Debbah, M.-S. Alouini, C. Yuen, J. D. Rosny, and S. Tretyakov, "Smart radio environments empowered by reconfigurable intelligent surfaces: How it works, state of research, and the road ahead," *IEEE Journal on Selected Areas in Communications*, Vol. 38, No. 11, 2450–2525, 2020.

[2] Bogale, T. E. and L. B. Le, "Massive MIMO and mmWave for 5G wireless HetNet: Potential benefits and challenges," *IEEE Vehicular Technology Magazine*, Vol. 11, No. 1, 64–75, 2016.

[3] Al-Ogaili, F. and R. M. Shubair, "Millimeter-wave mobile communications for 5G: Challenges and opportunities," in *2016 IEEE International Symposium on Antennas and Propagation (APSURSI)*, 1003–1004, Fajardo, PR, USA, 2016.

[4] Guo, Y. J., P.-Y. Qin, S.-L. Chen, W. Lin, and R. W. Ziolkowski, "Advances in reconfigurable antenna systems facilitated by innovative technologies," *IEEE Access*, Vol. 6, 5780–5794, 2018.

[5] Rangan, S., T. S. Rappaport, and E. Erkip, "Millimeter-wave cellular wireless networks: Potentials and challenges," *Proceedings of the IEEE*, Vol. 102, No. 3, 366–385, Mar. 2014.

[6] Lischke, S., D. Knoll, C. Mai, L. Zimmermann, A. Peczek, M. Kroh, A. Trusch, E. Krune, K. Voigt, and A. Mai, "High bandwidth, high responsivity waveguide-coupled germanium pin photodiode," *Optics Express*, Vol. 23, No. 21, 27 213–27 220, Mar. 2015.

[7] Zhao, S., Y. Luo, and N. Yan, "A low-profile anti-interference dual-port pattern reconfigurable monopole antenna for 5G applications," in *2022 IEEE 5th International Conference on Electronic Information and Communication Technology (ICEICT)*, 229–231, Hefei, China, 2022.

[8] Tang, S., Y. Zhang, J. Rao, T. Qiao, C.-Y. Chiu, and R. Murch, "Dual-port endfire millimeter wave reconfigurable antenna with optimized pixel surface," in *2023 IEEE International Symposium on Antennas and Propagation and USNC-URSI Radio Science Meeting (USNC-URSI)*, 969–970, Portland, OR, USA, 2023.

[9] Valizade Shahmirzadi, N. and H. Oraizi, "Design of reconfigurable coplanar waveguide-fed planar antenna for multiband multi-input-multi-output applications," *IET Microwaves, Antennas & Propagation*, Vol. 10, No. 14, 1591–1597, 2016.

[10] Zhang, Y., S. Tang, J. Rao, C.-Y. Chiu, X. Chen, and R. Murch, "A dual-port dual-beam pattern-reconfigurable antenna with independent 2-D beam-scanning," *IEEE Transactions on Antennas and Propagation*, Vol. 72, No. 10, 7628–7643, Oct. 2024.

[11] Zhang, Y., J. Geng, J. Lu, S. Yang, X. Tang, R. Zhao, A. Zhang, H. Li, X. Li, and E. Li, "A dual-port pattern reconfigurable antenna based on slot spoof surface plasmon polaritons," in *2023 IEEE 11th Asia-Pacific Conference on Antennas and Propagation (APCAP)*, 1–2, Guangzhou, China, 2023.

[12] Gao, K., Y. Zhou, T. Li, H. Yang, S. Li, and X. Cao, "Design of frequency-reconfigurable and decoupled dual-port single-radiating patch antennas using characteristic mode analysis," *IEEE Transactions on Antennas and Propagation*, Vol. 72, No. 9, 7068–7076, Sep. 2024.

[13] Farhan, M. J., "Reconfigurable a dual-port multi-band antenna system with high isolation tuning characteristics for portable wireless devices," *International Journal of Intelligent Engineering & Systems*, Vol. 14, No. 5, 7068–7076, 2021.

[14] Alekhya, B., N. A. Murugan, B. T. P. Madhav, and N. K. R. Reddy, "Millimeter-wave reconfigurable antenna for 5G wireless communications," *Progress In Electromagnetics Research Letters*, Vol. 101, 107–115, 2021.

[15] Zhou, Y., V. Basavarajappa, S. Alkaraki, and Y. Gao, "28 GHz millimeter wave multibeam antenna array with compact reconfigurable feeding network," in *2020 14th European Conference on Antennas and Propagation (EuCAP)*, 1–4, Copenhagen, Denmark, 2020.

[16] Yogeshwaran, A., "A multiple resonant microstrip patch heart shape antenna for satellite and Wi-Fi communication," *Analog Integrated Circuits and Signal Processing*, Vol. 121, No. 1, 1–11, 2024.

[17] Raheel, K., A. Altaf, A. Waheed, S. H. Kiani, D. A. Sehrai, F. Tubbal, and R. Raad, "E-shaped H-slotted dual band mmWave antenna for 5G technology," *Electronics*, Vol. 10, No. 9, 1019, 2021.

[18] Khan, A. and R. Nema, "Analysis of five different dielectric substrates on microstrip patch antenna," *International Journal of Computer Applications*, Vol. 55, No. 14, 0975–8887, 2012.

[19] Rabinovich, V. and N. Alexandrov, *Antenna Arrays and Automotive Applications*, Springer Science & Business Media, 2012.